Solar Energy Materials & Solar Cells 250 (2023) 112070

Contents lists available at ScienceDirect

Solar Energy Materials and Solar Cells

journal homepage: www.elsevier.com/locate/solmat

Cycling durability and potentiostatic rejuvenation of electrochromic tungsten oxide thin films: Effect of silica nanoparticles in $LiClO_4$–Propylene carbonate electrolytes

Gamze Atak [a,b], Sagar Ghorai [a], Claes G. Granqvist [a], Gunnar A. Niklasson [a], İlknur Bayrak Pehlivan [a,*]

[a] Department of Materials Science and Engineering, The Ångström Laboratory, Uppsala University, P.O. Box 35, SE-75103 Uppsala, Sweden
[b] Hacettepe University, Department of Physics Engineering, 06800 Beytepe, Ankara, Turkey

ARTICLE INFO

Keywords:
Electrochromism
Cycling durability
Potentiostatic rejuvenation
Tungsten oxide
Silica nanoparticles
Smart windows

ABSTRACT

Electrochromic (EC) technology allows control of the transmission of visible light and solar radiation through thin-film devices. When applied to "smart" windows, EC technology can significantly diminish energy use for cooling and air conditioning of buildings and simultaneously provide good indoor comfort for the buildings' occupants through reduced glare. EC "smart" windows are available on the market, but it is nevertheless important that their degradation under operating conditions be better understood and, ideally, prevented. In the present work, we investigated EC properties, voltammetric cycling durability, and potentiostatic rejuvenation of sputter-deposited WO_3 thin films immersed in $LiClO_4$–propylene carbonate electrolytes containing up to 3.0 wt% of ~7-nm-diameter SiO_2 nanoparticles. Adding about 1 wt% SiO_2 led to a significant improvement in cycling durability in the commonly used potential range of 2.0–4.0 V vs. Li/Li^+. Furthermore, X-ray photoemission spectroscopy indicated that O–Si bonds were associated with enhanced durability in the presence of SiO_2 nanoparticles.

1. Introduction

Energy efficiency in buildings stands out as particularly important for mitigating climate change, which is evident since the building sector is responsible for as much as ~36% of global energy use and ~39% of energy-related CO_2 emissions [1]. It should also be noted that, in the absence of effective means for improving energy efficiency, global energy consumption is forecast to grow by ~50% until 2050 [2]. Furthermore, most buildings have large windows and glass facades—jointly known as glazing—and means to improve those clearly can have an important impact on energy use. Dynamic or "smart" glazing, with variable optical properties, has been studied recently from an energy perspective, and it has been demonstrated that significant energy savings are indeed possible [3–6]; market research has identified electrochromic (EC) glazing as the most viable technology for dynamic glazing [7].

EC glazing contains materials that can change their optical properties in response to an external electrical voltage [8–11] and typically operate in contact with an ion conductor (electrolyte). The EC materials' coloration is called "cathodic" under ion insertion and "anodic" under ion extraction. EC glazing generally consists of a five-layer construction backed by a glass pane or positioned in a laminate configuration between glass panes. The construction comprises transparent conducting oxide (TCO) layer/cathodic EC layer/ion-conducting layer/anodic EC layer/TCO layer. Hence the central part of the five-layer arrangement is an ion conductor that, in a practical device, can be organic (an adhesive polymer) or inorganic (often based on an oxide film). This ion conductor is in contact with EC films, with WO_3 being a typical cathodic EC layer and NiO a typical anodic EC layer [8,12–15]. Using a fluid or a polymer electrolyte allows functionalization by adding non-scattering nanoparticles [16].

The mechanism for electrochromism in WO_3 films is generally explained by polaronic transitions between W^{5+} and W^{6+} states [17]. Specifically, electrons that enter to balance the charge of the inserted ions are localized at W^{5+} sites in the WO_3 and polarize their surrounding lattice to form small polarons. Incident photons, with energy $h\nu$, are absorbed by these small polarons as they hop from one site (A) to another site (B), according to [18]

* Corresponding author.
E-mail address: ilknur.bayrak_pehlivan@angstrom.uu.se (İ. Bayrak Pehlivan).

https://doi.org/10.1016/j.solmat.2022.112070
Received 1 May 2022; Received in revised form 29 September 2022; Accepted 15 October 2022
Available online 28 October 2022

$$h\nu + W^{5+}(A) + W^{6+}(B) \rightarrow W^{6+}(A) + W^{5+}(B)\ . \quad (1)$$

In heavily ion intercalated films, as well as in sub-stoichiometric films [19], W^{4+} sites can also contribute to the coloration.

Electrolytes play a vital role in the operation of EC systems and should provide high ion conductivity and optical transparency, minimum electronic conductivity, and compatibility with both cathode (WO_3) and anode (NiO). It has been reported that solid polymer electrolytes with added Li salts display relatively modest ion conductivity as most ions adhere to the polymer chains, but they show increased ionic conductivity when nanoparticles such as SiO_2, ZnO, TiO_2, or Al_2O_3 are incorporated [20–27]. It has also been found that the addition of SiO_2 nanoparticles can enhance the mechanical properties and electrochemical stability of polymer electrolytes. Another approach to improve polymer electrolytes' ionic conductivity is to add plasticizers such as propylene carbonate (PC), which provide lower viscosity and increase the flexibility in the polymeric segments, thereby improving ion mobility [28]. However, the plasticizers may diminish the mechanical and thermal stability of the electrolyte, which, in its turn, may be compensated by the addition of nanoparticles [29].

Cycling stability plays an important role in EC device performance and several methods have been examined to improve the stability of the devices [30,31]. One reason for the degradation of EC device performance is that trapping of Li^+ ions occurs during EC switching [32,33]. In 2015, a so-called rejuvenation method was applied to degraded EC films in order to recover their initial EC performance [32]. It has been conclusively shown that rejuvenation is due to extraction of trapped Li^+ ions from the EC WO_3 thin films [33]. Follow-up studies were carried out in either galvanostatic or potentiostatic mode as well as for other EC materials such as Ti and Mo oxides [14].

To the best of our knowledge, the effect of having nanoparticles in the electrolyte on cycling durability, degradation, and subsequent potentiostatic rejuvenation processes for EC materials has not been investigated before, although several other studies related to the rejuvenation of degraded EC thin films have been presented recently [32–36]. Therefore, we carried out an explorative study of a simplified system before contemplating a more complex electrolyte that may be of practical relevance—such as a mixture of salt, plasticizer, nanoparticles, and polymer. Thus, we added SiO_2 nanoparticles to a $LiClO_4$–PC electrolyte, which, in fact, appears to be the most common liquid electrolyte used for research on oxide-based EC materials. Specifically, we employed fumed silica, for which the SiO_2 surface was modified with hydroxyl groups so as to prevent particle clustering [37,38].

Below we report on cycling durability, degradation, and subsequent potentiostatic rejuvenation of WO_3 films immersed in $LiClO_4$–PC electrolyte to which up to 3.0 wt% of SiO_2 nanoparticles was added. X-ray diffractometry (XRD) and X-ray photoemission spectroscopy (XPS) were used to elucidate the influence of the SiO_2 nanoparticles.

2. Experimental techniques and procedures

2.1. Film preparation

The preparation of EC films of WO_3 requires judicious control of a number of deposition parameters [12,39]. Specifically, we used reactive DC magnetron sputtering in a multi-purpose deposition system based on a Balzers UTT 400 standard vacuum unit. The system was first maintained at 120 °C for 8 h, and a turbo molecular pump brought the base pressure to $\sim 6 \times 10^{-7}$ Torr. After this initial evacuation, Ar was introduced at a rate of 50 ml min^{-1}—using a mass-flow-controlled regulator—and pre-sputtering took place for 10 min to remove eventual contamination of the surface of a 5-cm-diameter W (purity 99.95%) target. Subsequently, Ar and O_2 (purities 99.998%) were entered at flow rates of 50 and 7.5 ml min^{-1}, respectively, while the total pressure was kept at 30 mTorr. Finally, the sputter power was set at 200 W. Depositions were performed on clean glass as well as on glass coated with transparent and electrically conducting indium–tin oxide (In_2O_3:Sn denoted ITO; sheet resistance 60 Ω). Substrate rotation gave the films a uniform thickness of 300 ± 20 nm as recorded by surface profilometry (DektakXT).

2.2. Electrolyte preparation and characterization

Electrolytes were prepared using $LiClO_4$ (purity 98%, Sigma Aldrich), PC ($C_4H_6O_3$, purity 99%, Sigma Aldrich), and fumed silica with a particle size of ~7 nm and surface area of 390 m^2/g (Sigma Aldrich). Specifically, 1 M $LiClO_4$ in PC was stirred at room temperature until the $LiClO_4$ was dissolved. Then, SiO_2 was added to the $LiClO_4$–PC in amounts of 0.5–3.0 wt% of the total solution, mixed for ~8 h at 75 °C, and subsequently cooled under continuous stirring until room temperature was reached. The long stirring time was chosen to guarantee uniform dispersion of nanoparticles in the electrolyte. Electrolytes were prepared inside a glovebox with humidity below ~0.5 ppm.

Spectral optical total and diffuse transmittance $T(\lambda)$ of electrolytes encased in a quartz cell, were recorded for $300 \leq \lambda \leq 2500$ nm by use of a PerkinElmer Lambda 900 spectrophotometer equipped with a $BaSO_4$-coated integrating sphere. The optical path length through the samples was 10 mm. The ionic conductivity was measured using a conductivity meter (SevenGo Duo SG78, Mettler Toledo).

2.3. Film characterization techniques

Structural characterization of the WO_3 films was performed at a grazing incidence angle of 1° with a Siemens D5000 diffractometer using $CuK_{\alpha 1}$ radiation at 1.5406 Å, 45 kV, and 40 mA in the 10–80° angular range using a step size of 0.02°.

XPS was conducted with a PHI Quantera II Scanning ESCA Microprobe operating with monochromatic Al $K_{\alpha 1}$ radiation and having a beam diameter of 100 μm. High-resolution scans were obtained with a pass energy of 26.00 eV and 0.05 eV resolution. Sample charging was avoided via a neutralizer filament. Before the XPS measurements, the films were taken out of the glove box, cleaned with isopropyl alcohol, and blown dry with compressed air. We did not do any ion etching before the high-resolution scans in order to preserve the surface properties of the film. Elemental depth profiles during sputter etching were obtained using a beam diameter of 200 μm and a pass energy of 224.00 eV. The C 1s peak was employed for energy calibration (284.8 eV). All XPS spectra were analyzed using CasaXPS software [40,41].

2.4. Electrochromic characterization

Electrochemical measurements by cyclic voltammetry (CV) were carried out in a three-electrode arrangement with a computer-controlled BioLogic Science Instruments SP-200 electrochemical interface. WO_3 films (~3.6 cm^2) were used as working electrodes, and Li foils were employed as counter and reference electrodes (sizes similar to those of the WO_3 films). For durability measurements on the WO_3 films, CV data were obtained for up to 500 cycles between 2.0 and 4.0 V, at a scan rate of 20 mV s^{-1}, in electrolytes comprised of $LiClO_4$–PC without or with added SiO_2 nanoparticles. All voltages are stated relative to a Li/Li^+ reference.

Potentiostatic treatments for rejuvenating degraded WO_3 thin films were performed using the same three-electrode configuration and in the same electrolytes by applying a voltage of 6.0 V for 20 h. Then, the samples were subjected to a zero-voltage "resting period" for 2 h to regain electrochemically stable conditions. Finally, CV data were taken for up to 300 cycles, as reported above, for rejuvenation assessment. All electrochemical and in-situ optical measurements were carried out in an Ar-filled glove box having water content below ~0.5 ppm.

In-situ optical measurements were performed with a set-up employing a light-emitting diode (LED) and a photodiode sensor. The LED produced green light with a maximum at $\lambda = 528$ nm, which is close

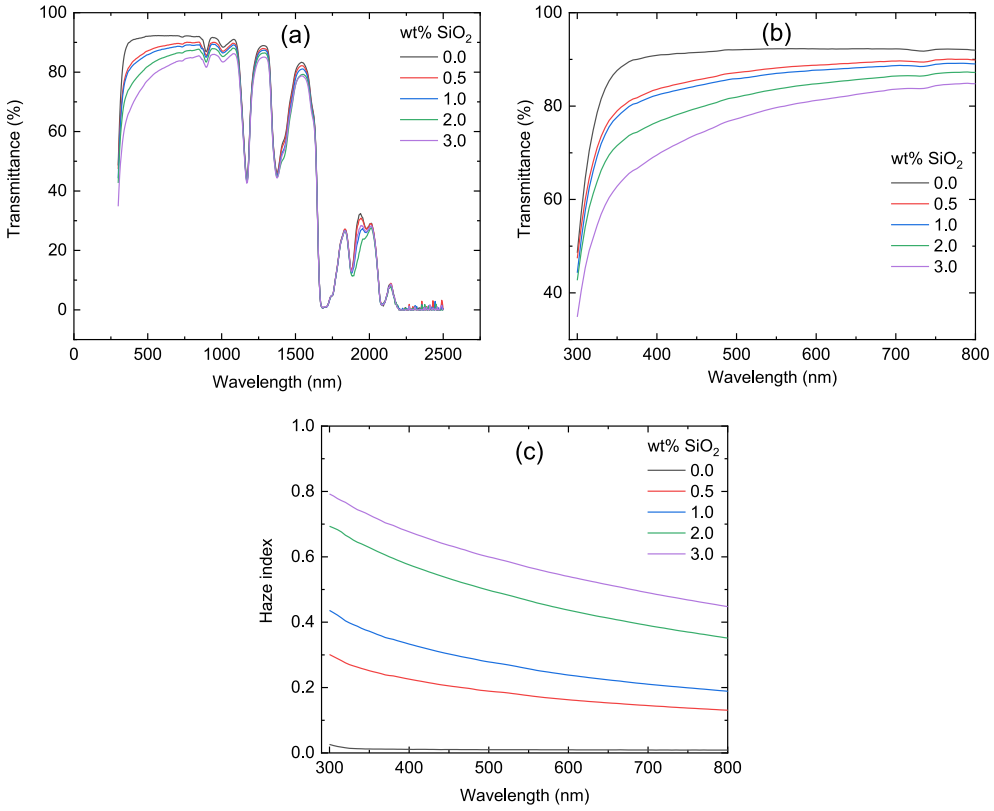

Fig. 1. Spectral optical transmittance (a) between 300 and 2500 nm, (b) with focus on the visible range and (c) haze index, for $LiClO_4$–PC electrolytes containing the shown amounts of ~7-nm-diameter SiO_2 nanoparticles. The optical path length of the samples used to measure the transmittance spectra of the electrolytes was 10 mm.

to the peak of the luminous spectrum, and with a full width at half maximum of 33 nm for the intensity distribution. The 100-%-level was obtained as the transmission of the cell containing nothing but electrolyte. Colored tungsten oxide films have a bluish appearance and the transmittance steadily decreases throughout the visible wavelength range, as shown in previous works from our group [14,42]. Measurements at our chosen wavelength, i.e., 528 nm, give a good approximation to the average luminous transmittance of the films.

EC properties were obtained from data on optical transmittance modulation ΔT given by

$$\Delta T = T_{bleached} - T_{colored} \, . \tag{2}$$

Inserted (−) and extracted (+) charge capacity Q was extracted from CV data according to

$$Q = \int (j \, dV) \Big/ s \, . \tag{3}$$

where j is current density, s is scan rate, and V is voltage. Combining optical and electrochemical data yielded coloration efficiency (CE) by

$$\mathrm{CE} = ln(T_{bleached}/T_{colored})/Q \, . \tag{4}$$

3. Results and discussion

The ion conductivity of the $LiClO_4$–PC-based electrolytes was found to be almost independent of their amount of SiO_2 nanoparticles lay in the range 4.90–5.14 μS m^{-1} as reported in Fig. S1 in Supporting Information (SI). An increase of ionic conductivity in polymer-based electrolytes with nanoparticles is well-known. In our case, similar ionic conductivity was obtained for the various concentrations of SiO_2 nanoparticles in the $LiClO_4$–PC since the plasticizers provide enhanced ionic conductivity thereby suppressing the contribution of nanoparticles on conductivity.

Spectral transmittance of the electrolyte is reported in Fig. 1a and shows high transmittance up to $\lambda \approx 850$ nm, whereas a number of absorption bands (transmittance minima) are apparent at longer wavelengths. The transmittance spectra of the electrolytes exhibited a decrease in transmittance at the visible range (Fig. 1b) with increasing SiO_2 content. The main influence of the SiO_2 nanoparticles is a continuous decrease of the transmittance as the wavelength is lowered. This effect is due to light scattering, as shown by measurements of the haze index (i.e., diffuse transmittance divided by total transmittance; Fig. 1c) which is enhanced as the SiO_2 content is increased. For example, at $\lambda =$ 528 nm, i.e., at the wavelength of interest for the results reported below, the transmittance decreased from 92 to 79% upon increasing the amount of SiO_2 nanoparticles as evident from Fig. S2 in SI.

3.1. Electrochemical and optical properties

Voltammetric cycling durability was investigated for the 2.0–4.0 V potential range before and after potentiostatic rejuvenation conducted as described above. Fig. 2a–e report cyclic voltammograms for WO_3 films immersed in $LiClO_4$–PC electrolytes with the shown amounts of SiO_2 nanoparticles. Cycling commenced at open-circuit potential and progressed as indicated. CV data are reported for cycle numbers 2, 300, and 500, after which the sample underwent potentiostatic rejuvenation; subsequent CV data are shown after 2 and 300 additional CV cycles. In many cases, the data for the initial cycles exhibited a secondary positive peak at about +3.75 V. The reason for this feature is not known,

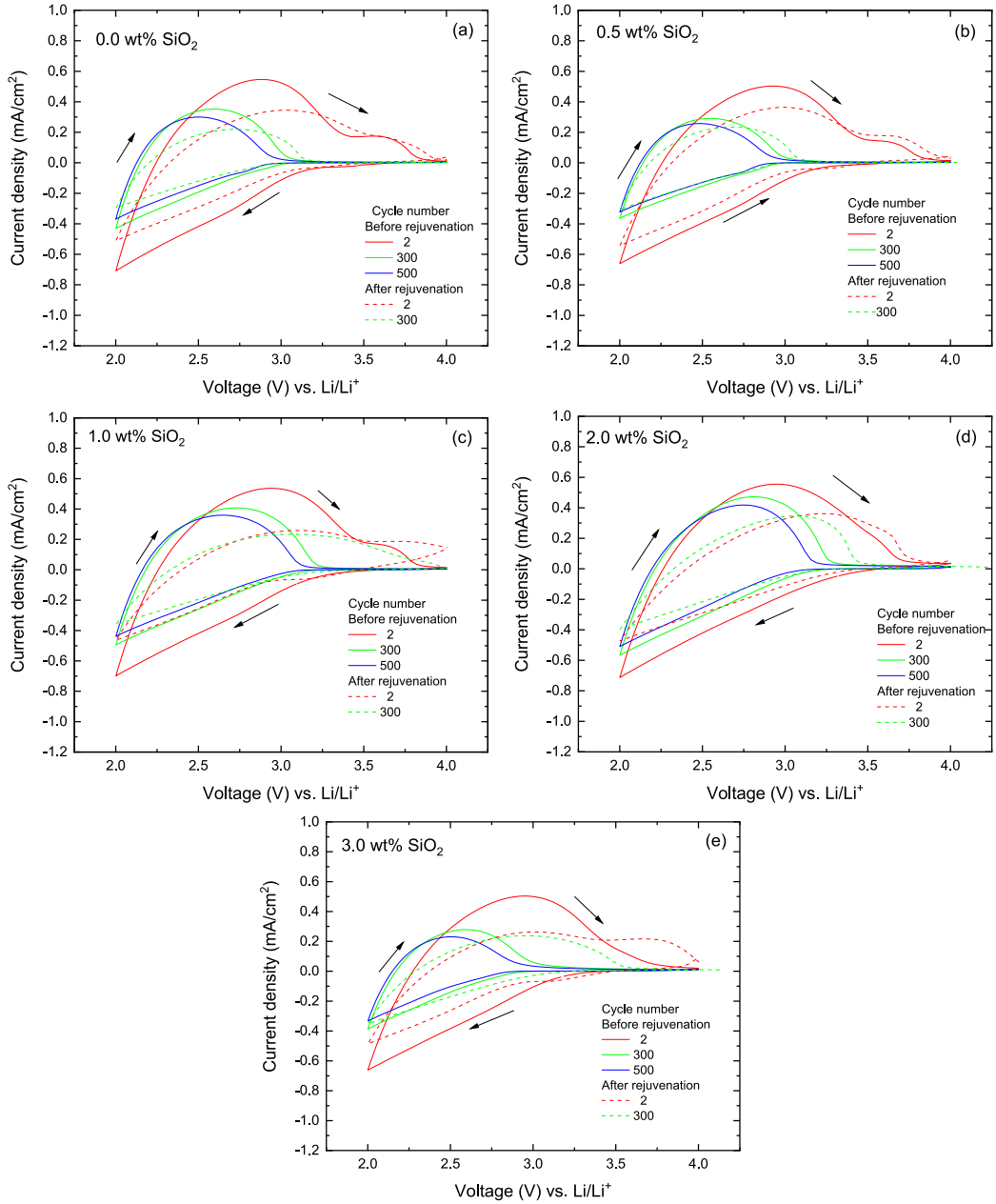

Fig. 2. Cyclic voltammograms for ~300-nm-thick WO_3 films immersed in electrolytes of $LiClO_4$–PC with the shown amounts of ~7-nm-diameter SiO_2 nanoparticles. Data are reported after the stated number of voltammetric cycles, at a scan rate of 20 mV s^{-1}, before and after potentiostatic rejuvenation as described in the main text. Arrows indicate scan directions for the cycling.

although it could be due to the release of Li ions from deep traps or maybe an effect of impurities in the electrolyte. Clearly, the shapes of all voltammograms, and their encircled areas signifying charge capacity, evolved pronouncedly during the CV cycling.

Corresponding data on the capacity for inserted and extracted charge are shown in Fig. 3a–e and on optical transmittance in bleached and colored states at $\lambda = 528$ nm in Fig. 3f–j, in both cases as a function of voltammetric cycle number. It is observed that Q decreased monotonically during CV cycling and, in general, was lower after potentiostatic rejuvenation than before rejuvenation at the same number of cycles. Voltammetric cycling also led to a monotonic increase in the colored-state transmittance of the WO_3 films, whereas the bleached-state transmittance remained almost unchanged. ΔT was higher before than after rejuvenation for the same cycle number. One important conclusion from Fig. 3 is that the potentiostatic rejuvenation procedure indeed led to a very significant restoration of both charge capacity and optical modulation, which is the expected result.

Fig. 3 presents a wealth of information, and Table 1 singles out a number of salient numbers on inserted charge density, coloration efficiency, and optical transmittance modulation at $\lambda = 528$ nm, specifically for the initial (second) and the final voltammetric cycle. Data are given before as well as after potentiostatic rejuvenation. It is evident that Q and ΔT show good co-variation, and the coloration efficiency (cf. Eq. (4)) is of the same order of magnitude and does not show any clear trends. It is evident that the addition of a small amount of SiO_2 nanoparticles increases the electrochemical durability both before and after potentiostatic rejuvenation, which is an important result and the main outcome of the present investigation. Optimum results were found for a SiO_2 nanoparticle content of 1 wt%, and neither lower nor larger amounts of SiO_2 gave as good results.

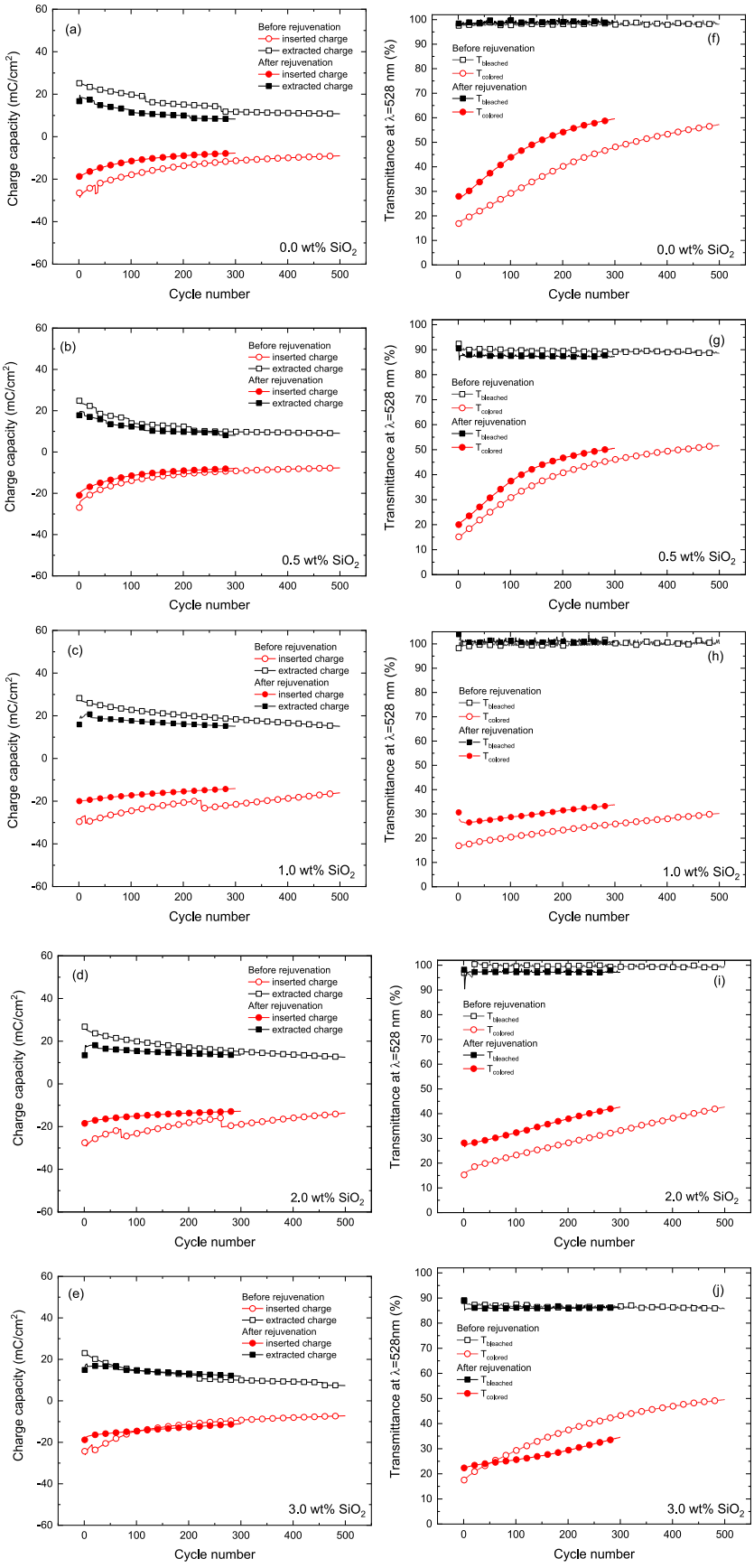

Fig. 3. Charge capacity (panels a–e) and optical transmittance T in colored and bleached states at a wavelength of 528 nm (panels f–j), in both cases vs voltammetric cycle number, for ~300-nm-thick WO_3 films immersed in electrolytes of $LiClO_4$–PC with the shown amounts of ~7-nm-diameter SiO_2 nanoparticles. Data are shown for voltammetric cycling, at a scan rate of 20 mV s^{-1}, for as-deposited films and after potentiostatic rejuvenation as described in the main text. Symbols denote data points and connecting lines were drawn for convenience.

Table 1
Inserted charge density, coloration efficiency, and optical modulation at a wavelength of 528 nm for ~300-nm-thick WO_3 films immersed in electrolytes of $LiClO_4$–PC with the shown amounts of ~7-nm-diameter SiO_2 nanoparticles. Data are given for the indicated numbers of voltammetric cycles, in the potential range 2.0–4.0 V (vs. Li/Li^+) at a scan rate of 20 mV s^{-1}, before and after potentiostatic rejuvenation as described in the main text.

SiO_2 content (wt %)	Inserted charge density before rejuvenation (mC cm^{-2})		Inserted charge density after rejuvenation (mC cm^{-2})		Coloration efficiency before rejuvenation (cm^2 C^{-1})		Coloration efficiency after rejuvenation (cm^2 C^{-1})		Optical modulation before rejuvenation (%)		Optical modulation after rejuvenation (%)	
	2^{nd} cycle	500^{th} cycle	2^{nd} cycle	300^{th} cycle	2^{nd} cycle	500^{th} cycle	2^{nd} cycle	300^{th} cycle	2^{nd} cycle	500^{th} cycle	2^{nd} cycle	300^{th} cycle
0.0	29	9	19	8	60.6	60.0	68.9	65.3	81	41	70	39
0.5	25	8	20	8	72.5	69.7	73.4	68.9	77	37	71	37
1.0	29	16	20	14	62.0	74.4	65.2	77.9	81	69	73	67
2.0	27	14	18	13	68.9	62.0	69.5	64.3	82	57	70	55
3.0	26	7	18	11	62.1	75.7	75.2	85.3	71	36	67	52

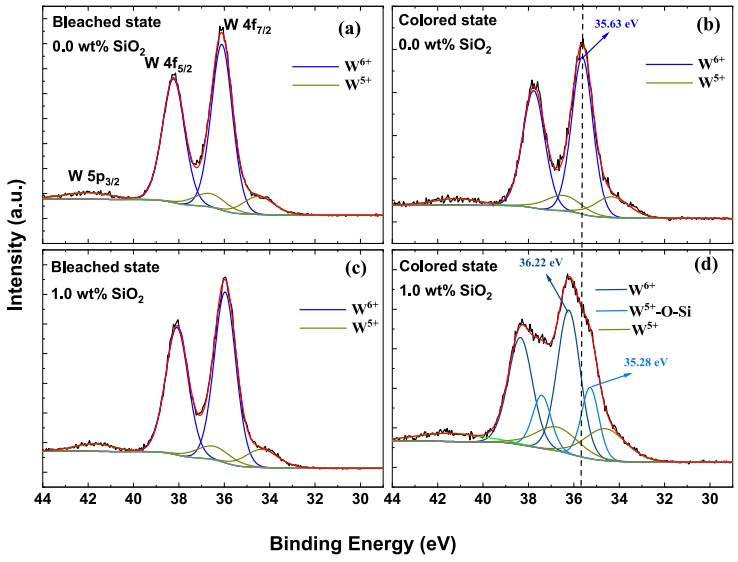

Fig. 4. XPS spectra in the energy range of the W $4f_{7/2}$ and W $4f_{5/2}$ peaks for WO_3 films after 100 voltammetric cycles in the 2.0–4.0-V range (vs. Li/Li^+) using a $LiCiO_4$–PC electrolyte without (upper panels) and with 1 wt% ~0.7-nm-diameter SiO_2 nanoparticles (lower panels). Data are shown for films in fully bleached (left-hand panels) and fully colored (right-hand panels) states. Experimental data and deconvoluted peaks are reported against the indicated background.

3.2. Structural and chemical-state properties

Structural characterisation was done using XRD in order to elucidate possible effects of the SiO_2 addition to the $LiClO_4$–PC electrolyte on the WO_3 thin films backed by ITO. Fig. S3 reports data for films in as-deposited state and after 100 CV cycles, performed in the same way as before, in electrolyte without and with 1.0 wt% of SiO_2 nanoparticles; the films were in their fully colored state. Fig. S3 shows a number of sharp diffraction peaks, all emanating from ITO, on a smoothly varying background. No distinct features could be assigned to the WO_3 films, which hence all were amorphous.

XPS was used to investigate the effect of the SiO_2 nanoparticles in the electrolyte on the coloration mechanism for the WO_3 thin films. Specifically, we recorded elemental depth profiles as well as high-resolution data for films colored and bleached during 100 CV cycles in $LiClO_4$–PC electrolytes without and with 1.0 wt% of SiO_2 nanoparticles. Depth profiling data are reported in Fig. S4 and, expectedly, showed clear signals due to W and O. After a sputtering time of several minutes, there was a distinct though a gradual increase of the signal from In, originating from the ITO film onto which the WO_3 film had been deposited, and a corresponding decrease of the signal from W. Additional weak signals can be seen due to C, Li, Sn, and, for the film cycled in the silica-containing electrolyte, also from Si. Fig. S5 shows that a significant Si signal was recorded only inside the WO_3 film that had been cycled in the electrolyte containing 1.0 wt% of SiO_2 nanoparticles. On the other hand, the noticeable increase in the intensity of Si 2p above 8 min of sputtering time comes from the glass substrate. It is conceivable that the SiO_2 nanoparticles in the electrolyte penetrate into the W-oxide-based film, but an influence from the glass substrate cannot be ruled out.

To further understand the coloration mechanism and the effect of the SiO_2 nanoparticle addition, XPS spectra of the W 4f state were deconvoluted by fitting to contributions from different oxidation states, as shown in Fig. 4. A void line shape [mixed Gaussian (70%)/Lorentzian (30%) function] and a Shirley-type background was used for XPS peak fitting [43,44]. Furthermore, instead of using the area ratio of the W4f doublets from their multiplicity ratio (1:1.3333), the more practical Scofield cross-section [45] (1:1.2721) was employed, as suggested by Sherwood [46]. Considering the super Coster-Kronig effect where two of the final-state holes are located in the same main shell as the initial vacancy, which results in a Lorentzian broadening of the corresponding core electron line [47], the width of the W $4f_{7/2}$ peak was set to 95% of the width of W $4f_{5/2}$ peak. The spin-orbital splitting energy (ΔE) for

Table 2
Binding energies for W $4f_{7/2}$, peak area, and corresponding spin-orbit splitting energy (ΔE) for W^{6+} and W^{5+} states, in WO_3 thin films colored and bleached during 100 voltammetric cycles in the 2.0–4.0-V range (vs. Li/Li^+) in $LiClO_4$–PC without and with 1.0 wt% of ~0.7-nm-diameter SiO_2 nanoparticles.

Sample state	wt% of SiO_2 in $LiClO_4$–PC	Binding energy of W $4f_{7/2}$ state (eV)			Peak area of W $4f_{7/2}$ state (%)			ΔE (eV)
		W^{6+}	Intermediate peak	W^{5+}	W^{6+}	Intermediate peak	W^{5+}	
As-deposited	–	36.20		34.93	93.85		6.15	2.14
Bleached	0.0	36.11		34.49	86.13		13.87	2.13
Colored	0.0	35.63		34.33	82.28		17.72	2.14
Bleached	1.0	35.96		34.35	86.14		13.86	2.12
Colored	1.0	36.22	35.28	34.61	56.42	21.22	22.36	2.13

Electrochromic coloration in WO_3 is associated with small polaron formation and the creation of W^{5+} states, as discussed in the Introduction (Eq. (1)). This effect is clearly seen in Fig. 4, where it can be observed by XPS that the W^{5+} peaks are more prominent in the colored films that had been cycled in the 2.0–4.0-V potential range.

every oxidation state, such as the binding energy difference between W^{6+} $4f_{7/2}$ and W^{6+} $4f_{5/2}$ and the difference between W^{5+} $4f_{7/2}$ and W^{5+} $4f_{5/2}$, were kept constant during the fitting process. It should be remembered that XPS is surface sensitive so that only a thin surface layer was probed, which necessitates caution in the interpretation of the XPS data. We note that surface impurities can be removed by sputtering the films with Ar ions, but this procedure may influence the oxidation states of W and hence was avoided here.

Table 2 lists extracted binding energies for W $4f_{7/2}$ and corresponding spin-orbit splitting energies. Clearly, two distinct oxidation states of W were observed, whose binding energies were in good agreement with previously reported values for W^{6+} [48–50] and W^{5+} [51–53]. Interestingly, the film colored at 2.0 V in the silica-containing electrolyte (Fig. 4d) yielded two peaks due to binding energies higher than that of W^{5+}. Gil-Rostra et al. [54] have reported peak splitting of this kind as originating from two different coordination states of the W ion. Specifically, for a given W^{n+} oxidation state the binding energy will increase by around 1 eV if the ion is in a W^{n+}-O-Si, configuration [54]. The observed binding energy of the W^{5+} state, in the colored film, varies between 34.3 and 34.6 eV. We therefore tentatively assign the peak at 35.28 eV to W^{5+}-O-Si. This result may indicate that some Si from the electrolyte is able to interact with the surface layers of the WO_3 film after extended cycling in the 2.0–4.0-V range. This notion is also consistent with the observation of a Si signal in the depth profiles of the film cycled in the electrolyte containing 1.0 wt% SiO_2 (Fig. S5).

4. Conclusion

We presented results of an explorative study on electrochromic films of WO_3 in Li-conducting electrolytes of $LiClO_4$–PC with additions of various amounts of SiO_2 nanoparticles. Voltammetric cycling durability of as-deposited and potentiostatically rejuvenated films was investigated for the commonly used 2.0–4.0-V range vs. Li/Li^+. It was found that the addition of about 1 wt% of ~0.7-nm-diameter SiO_2 nanoparticles consistently led to improved durability. XPS studies provided evidence that this beneficial effect was associated with O–Si coordination, possibly connected to the presence of a solid-electrolyte interphase such as the one commonly found in Li-ion batteries [55].

Our results show that nanoparticles added to the electrolyte in an electrochromic device present a novel avenue towards the creation of superior voltammetric cycling durability. Nanoparticles are also able to give multifunctionality for such devices, as noted in the Introduction, one example being that ITO nanoparticles can efficiently block the transmittance of infrared solar radiation [16]. It is evident that various synergies can be accomplished by the use of nanoparticles in the electrolyte of electrochromic devices such as "smart" windows. This is a feature worthy of further scientific inquiry and may also have an important impact on the design of other types of energy-related devices.

CRediT authorship contribution statement

Gamze Atak: Writing – review & editing, Writing – original draft, Methodology, Investigation, Formal analysis. **Sagar Ghorai:** Writing – review & editing, Methodology, Investigation, Formal analysis. **Claes G. Granqvist:** Writing – review & editing, Supervision. **Gunnar A. Niklasson:** Writing – review & editing, Supervision. **İlknur Bayrak Pehlivan:** Writing – review & editing, Writing – original draft, Supervision, Resources, Conceptualization.

Declaration of competing interest

The authors declare that they have no known competing financial interests or personal relationships that could have appeared to influence the work reported in this paper.

Data availability

Data will be made available on request.

Acknowledgments

We acknowledge Myfab Uppsala for providing facilities and experimental support. Myfab is funded by the Swedish Research Council (2019–00207) as a national research infrastructure. Gamze Atak wants to thank the Scientific and Technological Research Council of Turkey (TÜBİTAK) for financial support to work at Uppsala University.

Appendix A. Supplementary data

Supplementary data to this article can be found online at https://doi.org/10.1016/j.solmat.2022.112070.

References

[1] U.N. Environment, International Energy Agency, Towards a Zero-Emission, Efficient, and Resilient Buildings and Construction Sector: Global Status Report 2017, United Nations & International Energy Agency, New York, U.S.A. & Paris, France, 2017.
[2] International Energy Agency, Transition to Sustainable Buildings: Strategies and Opportunities to 2050, International Energy Agency, Paris, France, 2013.
[3] F. Favoino, M. Overend, Q. Jin, The optimal thermo-optical properties and energy savings potential of adaptive glazing technologies, Appl. Energy 156 (2015) 1–15, https://doi.org/10.1016/j.apenergy.2015.05.065.
[4] A. Cannavale, F. Martellotta, P. Cossari, G. Gigli, U. Ayr, Energy savings due to building integration of innovative solid-state electrochromic devices, Appl. Energy 225 (2018) 975–985, https://doi.org/10.1016/j.apenergy.2018.05.034.
[5] J. Chambers, P. Hollmuller, O. Bouvard, A. Schueler, J.-L. Scartezzini, E. Azar, M. K. Patel, Evaluating the electricity savings potential of electrochromic glazing for cooling and lighting at the scale of the Swiss non-residential national building stock using a Monte Carlo method, Energy 185 (2019) 136–147, https://doi.org/10.1016/j.energy.2019.07.037.
[6] R. Tällberg, B.P. Jelle, R. Loonen, T. Gao, M. Hamdy, Comparison of the energy saving potential of adaptive and controllable smart windows: a state-of-the-art review and simulation studies of thermochromic, photochromic and electrochromic technologies, Sol. Energy Mater. Sol. Cells 200 (2019) 109828, https://doi.org/10.1016/j.solmat.2019.02.041.

[7] Smart Windows Market: 2018–2027, n-Tech Research, Glen Allen, VA, USA, 2018.
[8] C.G. Granqvist, Handbook of Inorganic Electrochromic Materials, Elsevier, Amsterdam, The Netherlands, 1995.
[9] R.J. Mortimer, D.R. Rosseinsky, P.M.S. Monk (Eds.), Electrochromic Materials and Devices, Wiley-VCH, Weinheim, Germany, 2015.
[10] J.W. Xu, Electrochromic Smart Materials: Fabrication and Applications, Royal Society of Chemistry, Cambridge, UK, 2019.
[11] F.A. da Silveira, A. Parisotto, F. Amorim Berutti, A. Kopp Alves, Electrochromic nanomaterials, in: A. Kopp Alves (Ed.), Technological Applications of Nanomaterials, Springer, Berlin Heidelberg, Germany, 2022, pp. 135–152.
[12] C.G. Granqvist, Electrochromics for smart windows: oxide-based thin films and devices, Thin Solid Films 564 (2014) 1–38, https://doi.org/10.1016/j.tsf.2014.02.002.
[13] G.A. Niklasson, C.G. Granqvist, Electrochromics for smart windows: thin films of tungsten oxide and nickel oxide, and devices based on these, J. Mater. Chem. 17 (2007) 127–156, https://doi.org/10.1039/b612174h.
[14] C.G. Granqvist, M.A. Arvizu, İ. Bayrak Pehlivan, H.-Y. Qu, R.-T. Wen, Electrochromic materials and devices for energy efficiency and human comfort in buildings: a critical review, Electrochim. Acta 259 (2018) 1170–1183, https://doi.org/10.1016/j.electacta.2017.11.169.
[15] C.G. Granqvist, İ. Bayrak Pehlivan, G.A. Niklasson, Electrochromics on a roll: web-coating and lamination for smart windows, Surf. Coat. Technol. 336 (2018) 133–138, https://doi.org/10.1016/j.surfcoat.2017.08.006.
[16] İ. Bayrak Pehlivan, R. Marsal, E. Pehlivan, E.L. Runnerstrom, D.J. Milliron, C. G. Granqvist, G.A. Niklasson, Electrochromic devices with polymer electrolytes functionalized by SiO_2 and In_2O_3:Sn nanoparticles: rapid coloring/bleaching dynamics and strong near-infrared absorption, Sol. Energy Mater. Sol. Cells 126 (2014) 241–247, https://doi.org/10.1016/j.solmat.2013.06.010.
[17] O.F. Schirmer, V. Wittver, G. Baur, G. Brandt, Dependence of WO_3 electrochromic absorption on crystallinity, J. Electrochem. Soc. 124 (1977) 749–753, https://doi.org/10.1149/1.2133399.
[18] C.A. Triana, C.G. Granqvist, G.A. Niklasson, Electrochromics and small-polaron hopping in oxygen deficient and lithium intercalated amorphous tungsten oxide films, J. Appl. Phys. 118 (2015) 024901, https://doi.org/10.1063/1.4926488.
[19] S.-H. Lee, H.M. Cheong, J.-G. Zhang, A. Mascarenhas, D.K. Benson, S.K. Deb, Electrochromic mechanism in a-WO_{3-y} thin films, Appl. Phys. Lett. 74 (1999) 242–244, https://doi.org/10.1063/1.123268.
[20] F. Croce, G.B. Appetecchi, L. Persi, B. Scrosati, Nanocomposite polymer electrolytes for lithium batteries, Nature 394 (1998) 456–458, https://doi.org/10.1038/28818.
[21] F. Croce, R. Curini, A. Martinelli, L. Persi, F. Ronci, B. Scrosati, R. Caminiti, Physical and chemical properties of nanocomposite polymer electrolytes, J. Phys. Chem. B 103 (1999) 10632–10638, https://doi.org/10.1021/jp992307u.
[22] J.-H. Ahn, G.X. Wang, H.K. Liu, S.X. Dou, Nanoparticle-dispersed PEO polymer electrolytes for Li batteries, J. Power Sources 119-121 (2003) 422–426, https://doi.org/10.1016/S0378-7753(03)00264-7.
[23] M. Wachtler, D. Ostrovskii, P. Jacobsson, B. Scrosati, A study on PVdF-based SiO_2-containing composite gel-type polymer electrolytes for lithium batteries, Electrochim. Acta 50 (2004) 357–361, https://doi.org/10.1016/j.electacta.2004.01.103.
[24] S. Ahmad, S. Ahmad, S.A. Agnihotry, Nanocomposite electrolytes with fumed silica in poly(methyl methacrylate): thermal, rheological and conductivity studies, J. Power Sources 140 (2005) 151–156, https://doi.org/10.1016/j.jpowsour.2004.08.002.
[25] Y.- J.- Wang, D. Kim, Crystallinity, morphology, mechanical properties and conductivity study of in situ formed PVdF/$LiClO_4$/TiO_2 nanocomposite polymer electrolytes, Electrochim. Acta 52 (2007) 3181–3189, https://doi.org/10.1016/j.electacta.2006.09.070.
[26] İ. Bayrak Pehlivan, C.G. Granqvist, R. Marsal, P. Georén, G.A. Niklasson, [PEI–SiO_2]:[LiTFSI] nanocomposite polymer electrolytes: ion conduction and optical properties, Sol. Energy Mater. Sol. Cells 98 (2012) 465–471, https://doi.org/10.1016/j.solmat.2011.11.021.
[27] D. Zhou, R. Zhou, C. Chen, W.-A. Yee, J. Kong, G. Ding, X. Lu, Non-volatile polymer electrolyte based on poly(propylene carbonate), ionic liquid, and lithium perchlorate for electrochromic devices, J. Phys. Chem. B 117 (2013) 7783–7789, https://doi.org/10.1021/jp4021678.
[28] H.M.J.C. Pitawala, M.A.K.L. Dissanayake, V.A. Seneviratne, B.-E. Mellander, I. Albinson, Effect of plasticizers (EC or PC) on the ionic conductivity and thermal properties of the $(PEO)_9LiTf$: Al_2O_3 nanocomposite polymer electrolyte system, J. Solid State Electrochem. 12 (2008) 783–789, https://doi.org/10.1007/s10008-008-0505-7.
[29] G. Hirankumar, N. Mehta, Effect of incorporation of different plasticizers on structural and ion transport properties of PVA-$LiClO_4$ based electrolytes, Heliyon 4 (2018), e00992, https://doi.org/10.1016/j.heliyon.2018.e00992.
[30] I.-G. Choi, D. Choi, J.-Y. Lee, M. Lee, S.-I. Park, D.-M. Chun, C.S. Lee, W.-S. Chu, One million cycle durability test of electrochromic devices using charge balance control, Int. J. Precis. Eng. Manuf.-Green Technol. 7 (2020) 195–203, https://doi.org/10.1007/s40684-019-00153-x.
[31] M. Lee, M. Son, D.-M. Chun, C.S. Lee, Evaluation of electrochromic device influenced by various formulation of solid polymer electrolyte, Int. J. Precis. Eng. Manuf. 22 (2021) 189–199, https://doi.org/10.1007/s12541-020-00451-4.
[32] R.-T. Wen, C.G. Granqvist, G.A. Niklasson, Eliminating degradation and uncovering ion-trapping dynamics in electrochromic WO_3 thin films, Nat. Mater. 14 (2015) 996–1001, https://doi.org/10.1038/nmat4368.
[33] M.A. Arvizu, R.-T. Wen, D. Primetzhofer, J.E. Klemberg-Sapieha, L. Martinu, G. A. Niklasson, C.G. Granqvist, Galvanostatic ion detrapping rejuvenates oxide thin films, ACS Appl. Mater. Interfaces 7 (2015) 26387–26390, https://doi.org/10.1021/acsami.5b09430.
[34] C.G. Granqvist, M.A. Arvizu, H.-Y. Qu, R.-T. Wen, G.A. Niklasson, Advances in electrochromic device technology: multiple roads towards superior durability, Surf. Coatings Technol. 357 (2019) 619–625, https://doi.org/10.1016/j.surfcoat.2018.10.048.
[35] İ. Sorar, E.A. Rojas-González, İ. Bayrak Pehlivan, C.G. Granqvist, G.A. Niklasson, Electrochromism of W–Ti oxide thin films: cycling durability, potentiostatic rejuvenation, and modelling of electrochemical degradation, J. Electrochem. Soc. 166 (2019) H795–H801, https://doi.org/10.1149/2.0421915jes.
[36] İ. Sorar, İ. Bayrak Pehlivan, J. Bohlin, C.G. Granqvist, G.A. Niklasson, Potentiostatic rejuvenation of electrochromic WO_3 thin films: exploring the effect of polyethylene oxide in $LiClO_4$–propylene carbonate electrolytes, Sol. Energy Mater. Sol. Cells 218 (2020) 110767, https://doi.org/10.1016/j.solmat.2020.110767.
[37] P.M. Price, J.H. Clark, D.J. Macquarrie, Modified silicas for clean technology, J. Chem. Soc. Dalton Trans. 2 (2000) 101–110, https://doi.org/10.1039/A905457J.
[38] P.A.R.D. Jayathilaka, M.A.K.L. Dissanayake, I. Albinsson, B.-E. Mellander, Effect of nano-porous Al_2O_3 on thermal, dielectric and transport properties of the $(PEO)_9LiTFSI$ polymer electrolyte system, Electrochim. Acta 47 (2002) 3257–3268, https://doi.org/10.1016/S0013-4686(02)00243-8.
[39] G. Atak, İ. Bayrak Pehlivan, J. Montero, C.G. Granqvist, G.A. Niklasson, Electrochromic tungsten oxide films prepared by sputtering: optimizing cycling durability by judicious choice of deposition parameters, Electrochim. Acta 367 (2021) 137233, https://doi.org/10.1016/j.electacta.2020.137233.
[40] N. Fairley, CasaXPS, Version 2.3.23PR1.0, Casa Software Ltd., Teignmouth, U.K., 2020.
[41] N. Fairley, V. Fernandez, M. Richard-Plouet, C. Guillot-Deudon, J. Walton, E. Smith, D. Flahaut, M. Greiner, M. Biesinger, S. Tougaard, D. Morgan, J. Baltrusaitis, Systematic and collaborative approach to problem solving using X-ray photoelectron spectroscopy, Appl. Surf. Sci. Adv. 5 (2021) 100112, https://doi.org/10.1016/j.apsadv.2021.100112.
[42] R.-T. Wen, M.A. Arvizu, M. Morales-Luna, C.G. Granqvist, G.A. Niklasson, Ion trapping and detrapping in amorphous tungsten oxide thin films observed by real-time electro-optical monitoring, Chem. Mater. 28 (2016) 4670–4676, https://doi.org/10.1021/acs.chemmater.6b01503.
[43] D.A. Shirley, High-resolution x-ray photoemission spectrum of the valence bands of gold, Phys. Rev. B5 (1972) 4709–4714, https://doi.org/10.1103/PhysRevB.5.4709.
[44] J.E. Castle, H. Chapman-Kpodo, A. Proctor, A.M. Salvi, Curve-fitting in XPS using extrinsic and intrinsic background structure, J. Electron. Spectrosc. Relat. Phenom. 106 (2000) 65–80, https://doi.org/10.1016/s0368-2048(99)00089-4.
[45] J.H. Scofield, Hartree-Slater subshell photoionization cross-sections at 1254 and 1487 eV, J. Electron. Spectrosc. Relat. Phenom. 8 (1976) 129–137, https://doi.org/10.1016/0368-2048(76)80015-1.
[46] P.M.A. Sherwood, The use and misuse of curve fitting in the analysis of core X-ray photoelectron spectroscopic data, Surf. Interface Anal. 51 (2019) 589–610, https://doi.org/10.1002/sia.6629.
[47] N. Mårtensson, R. Nyholm, Electron spectroscopic determinations of M and N core-hole lifetimes for the elements Nb–Te (Z = 41–52), Phys. Rev. B24 (1981) 7121–7134, https://doi.org/10.1103/PhysRevB.24.7121.
[48] P. Biloen, G.T. Pott, X-ray photoelectron spectroscopy study of supported tungsten oxide, J. Catal. 30 (1973) 169–174, https://doi.org/10.1016/0021-9517(73)90063-8.
[49] T.H. Fleisch, G.J. Mains, An XPS study of the UV reduction and photochromism of MoO_3 and WO_3, J. Chem. Phys. 76 (1982) 780–786, https://doi.org/10.1063/1.443047.
[50] P.G. Gassman, D.W. Macomber, S.M. Willging, Isolation and characterization of reactive intermediates and active catalysts in homogeneous catalysis, J. Am. Chem. Soc. 107 (1985) 2380–2388, https://doi.org/10.1021/ja00294a031.
[51] L. Su, H. Wang, Z. Lu, All-solid-state electrochromic window of Prussian blue and electrodeposited WO_3 film with poly(ethylene oxide) gel electrolyte, Mater. Chem. Phys. 56 (1998) 266–270, https://doi.org/10.1016/S0254-0584(98)00141-2.
[52] L. Weinhardt, M. Blum, M. Bär, C. Heske, B. Cole, B. Marsen, E.L. Miller, Electronic surface level positions of WO_3 thin films for photoelectrochemical hydrogen production, J. Phys. Chem. C 112 (2008) 3078–3082, https://doi.org/10.1021/jp7100286.
[53] M. Vasilopoulou, A. Soultati, D.G. Georgiadou, T. Stergiopoulos, L.C. Palilis, S. Kennou, N.A. Stathopoulos, D. Davazoglou, P. Argitis, Hydrogenated under-stoichiometric tungsten oxide anode interlayers for efficient and stable organic photovoltaics, J. Mater. Chem. A 2 (2014) 1738–1749, https://doi.org/10.1039/c3ta13975a.
[54] J. Gil-Rostra, M. Cano, J.M. Pedrosa, F.J. Ferrer, F. García-García, F. Yubero, A. R. González-Elipe, Electrochromic behavior of $W_xSi_yO_z$ thin films prepared by reactive magnetron sputtering at normal and glancing angles, ACS Appl. Mater. Interfaces 4 (2012) 628–638, https://doi.org/10.1021/am2014629.
[55] P. Verma, P. Maire, P. Novák, A review of the features and analyses of the solid electrolyte interphase in Li-ion batteries, Electrochim. Acta 55 (2010) 6332–6341, https://doi.org/10.1016/j.electacta.2010.05.072.